Hindawi
Mathematical Problems in Engineering
Volume 2020, Article ID 5489896, 20 pages
https://doi.org/10.1155/2020/5489896

Research Article

Research on Theoretical Modeling and Parameter Sensitivity of a Single-Rod Double-Cylinder and Double-Coil Magnetorheological Damper

Suojun Hou[1,2] **and Gang Liu**[1]

[1]*School of Vehicle and Traffic Engineering, Henan Institute of Technology, Xinxiang 453000, China*
[2]*China Automotive Technology and Research Center Co., Ltd., Tianjin 300300, China*

Correspondence should be addressed to Suojun Hou; 149584484@qq.com

Received 14 September 2019; Revised 27 December 2019; Accepted 13 January 2020; Published 10 February 2020

Academic Editor: Sergey A. Suslov

For the single-rod double-cylinder and double-coil magnetorheological (MR) damper studied in this paper, the damping force model of the damper is established by adopting multidisciplinary domain modeling method bond graph theory. Firstly, combined with the structure of the MR damper, the bond graph model of the MR damper was established, the damping force model of the damper was derived through the bond graph theory, and the influence factors, such as the displacement, velocity, and acceleration of the damper were considered in the model. Based on the simulation of force-displacement and force-velocity characteristics of the damping force carried out by the damper theoretical model under different currents and velocities as well as the comparison with the damper bench test results, it was found that the force-displacement and force-velocity characteristic experiment curves of the damper agreed well with the simulation results. Under different working conditions, the maximum error of damping force of the MR damper was 7.2%. The damping force model of the MR damper studied in this paper was compared with that of the damper without considering the inertia force of MR fluid, and the influence of the inertia force of MR fluid on the damping force of the MR damper was analyzed. The results show that when the frequency of the damper is large, the inertial force of MR fluid has an important influence on the damping force; therefore, considering the inertial force of MR fluid in the model can greatly improve the accuracy of the model. The influence degree of key parameters on the damping force of the MR damper was studied through the theoretical model; such key parameters ranging from large to small were the channel clearance, energizing current, piston diameter, motion velocity, channel length, zero-field viscosity of MR fluid, and nitrogen pressure. This provides a basis for the adjustment of the damping force of the MR damper.

1. Introduction

The main function of the automobile suspension system is to baffle vibration from different pavements. A good suspension system can effectively screen vibrations from different pavements and improve the steering stability of automobile at the same time [1, 2]. Automotive suspension has experienced the development stages of passive suspensions, semiactive suspensions, and fully active suspensions [3–5]. Among them, the semiactive suspension is characterized by not changing the stiffness of the suspension, only changing the damping of the suspension damper, and consuming almost no vehicle-driving power during operation, and its vibration damping performance is between the passive suspension and the fully active suspension. Therefore, the semiactive suspension system has become the main development trend of the suspension system [6].

The semiactive suspension of the MR damper utilizes the controllable characteristics of MR fluid viscosity to achieve continuous adjustment of the damping force, to meet the requirements of vibration reduction under different driving conditions, and to effectively improve the steering stability of automobile [7–11].

At present, various models of MR damper have been put forward by scholars from different countries, mainly including

parametric model, nonparametric model, and physical model. Based on the viscoelastic-plastic properties of MR fluid, the parametric model takes the MR damper as a combination of elastic and damping elements according to different constitutive models and directly speculates its physical model based on the observed characteristics of things. Most of the parameters are of physical meaning, and still experimental tests are needed to identify them, such as the Bingham viscoplastic model, the biviscous-based parametric model, and Bouc–Wen and its modified models. The nonparametric model, of which parameters are of no physical meaning, finds a mathematical function with similar characteristics to establish the mathematical model of the MR damper according to the characteristics of the result curve of MR damper experimental tests; test data are needed for parameter identification, such as polynomial model, neural network model, and fuzzy neural model. The physical model refers to the damper damping force model derived completely from physical laws, and each parameter has a clear physical meaning, such as the structure parameters of damper, the performance parameters of MR fluid, the turns per coil, and the magnetic field intensity applied; test data are not necessary for parameter identification, and there is relatively few research on this model at home and abroad.

In 1987, Stanway et al. established a dynamic damping force model of MR damper based on the MR fluid constitutive relationship of the Bingham viscoplastic model [12].

In 2005, Hong et al. of Inha University, South Korea [13, 14], proposed a dimensionless Bingham MR damper model in the mixed mode, which was verified to be corrected through experiments.

In order to describe the preyield hysteresis properties of MR fluid, Wereley et al. [15] proposed a damping force model in 1998 based on biviscous MR constitutive relationship, which well described the velocity hysteresis properties of the MR damper.

Research studies found that shear thickening and thinning occur in the MR fluid. In 1999, Wang and Gordaninejad [16] and Lee et al. [17] adopted the Herschel–Bulkley model, which could describe the shear thickening and thinning of the MR fluid, to describe the mechanical model of MR device.

In 1997, Spencer et al. [18] described the preyield elastic properties and the postyield plastic properties of MR fluid through the combination of springs and damping elements in series and parallel and derived the viscoelastic-plastic Bouc–Wen model that could describe the hysteresis properties of the MR damper.

In 2001, Choi [19] of Inha University, South Korea, analyzed the property of dependency on magnetic field in the Bingham, Bouc–Wen, and biviscous models, proposed the polynomial model of the MR damper used in medium-sized passenger vehicles to improve the control performance, and designed and manufactured the samples of the MR damper; the model was verified to be corrected by the characteristic tests of damper.

In 2002, Yao et al. [20] of Nanyang Technological University, Singapore, designed a single-rod single-cylinder MR damper; the performance of the MR fluid damper was predicted by using the Bouc–Wen model; the force-displacement curve was obtained, and the equivalent damping coefficient of the damper was obtained through the MATLAB optimization method and experimental results.

In 2011, Komatsu et al. [21] of Kanazawa University, Japan, studied two types of single-rod single-cylinder MR dampers with different damping forces, established the Bouc–Wen damping force model of the damper, and studied the effect of controlling its pitch and roll motion on a small racing car through MATLAB.

In 2005, Du et al. of Imperial College London, England, and Sze and Lam of the University of Hong Kong [22] established a polynomial model to describe the relationship between damping force and current and velocity, and this model could well describe the external properties of damper.

In 2008, Dominguez et al. [23] of Mexico, based on Bouc–Wen model, established a new nonlinear model of MR damper containing the amplitude values of frequency, current, and excitation, and this model could well describe the hysteresis properties of damper.

In 2008, Bajkowski [24] of Warsaw University of Technology, Poland, studied the theoretical model of MR damper containing the temperature effects.

In 2011, Boada et al. [25] of Spain studied a method based on the network structural recursion to calculate the damping force of the MR damper.

In 2009, Yao of Nanjing Forestry University, China [26], conducted the characteristic tests on the MR damper and proposed a composite polynomial model containing the parameters of frequency and amplitude.

In 2011, Guan et al. [27] of Harbin Institute of Technology, China, studied the modeling and hysteresis properties of the MR damper.

In 2011, Guo [28] of Harbin Institute of Technology, China, studied MR damper from the following five aspects: fluid constitutive model, quasistatic mechanical model, transient response of damper, multiobjective optimization and design, and hysteresis properties of damper and dynamic design.

Other nonparametric models studied by scholars at home and abroad mainly include neural network model [29–31] and fuzzy neural model [32–34], and these models generally have the characteristics of strong robustness and high accuracy.

Lee and Choi [35] adopted the bond graph theory to establish a physical model of MR damper containing the piston motion displacement, the piston velocity, and yield stress of MR fluid while neglecting the inertial force of MR fluid, as shown in the following formula:

$$F_e = k_e x_p + c_e \dot{x}_p + P_{\mathrm{MR}} \mathrm{sgn}\left(\dot{x}_p\right), \tag{1}$$

where $k_e = (A_r^2/C_g)$, $c_e = (A_p - A_r)^2 (12\eta L/2\pi r h^3)$, and $P_{\mathrm{MR}} = 4(A_p - A_r)(2L_m/h_m)\alpha H^{\beta}$.

In the above equation, variables are defined as follows: k_e, equivalent stiffness coefficient; c_e, equivalent damping coefficient; P_{MR}, yield stress of MR fluid; x_p, piston displacement; $\dot{x}_p$, piston velocity; A_p, piston area; A_r, piston rod area; C_g, gas compliance in the gas chamber; η, viscosity of MR fluid; L, length of the inner cylinder; r, outer radius of

the inner cylinder; h, gap between the inner and outer cylinders; L_m, length of magnetic pole; h_m, gap between the magnetic poles; and H, magnetic field.

In this paper, firstly, a single-rod double-cylinder and double-coil MR damper is designed. Then, the physical model of MR damper is established based on the multi-domain modeling theory, i.e., the bond graph modeling theory. Finally, the correctness of the model is proved by the bench test. The theoretical model is used to study the influence of key parameters on the damping force of the MR damper.

This paper makes an innovation by concluding not only the piston motion displacement, velocity, and shear stress of MR fluid but also the acceleration term, which represents the inertial force of MR fluid flow and analyzes the influence of MR fluid inertial force on the damping force of the MR damper under different working conditions.

2. Structural Design of MR Damper

2.1. Structure and Principle of MR Damper. The MR damper is classified into the single-rod single-cylinder and single-coil type, single-rod double-cylinder and single-coil type, and other types. In order to increase the damping force of the damper, the damping channel and energizing coil were separately arranged at the upper and lower ends of the damper. In this paper, a single-rod double-cylinder and double-coil MR damper was studied and the structure is shown in Figure 1.

When the MR damper was in the stretching stroke, the piston (30) and piston rod (35) drove the MR fluid in the recovery chamber (31) at the upper part of the piston (30) to flow upward, and the MR fluid was squeezed into the upper end annular damping channel (6) under the action of the pressure, entered the compensation chamber (17) between the inner and outer cylinders, and then flowed into the compression chamber (28) below the piston (30) through the lower end annular damping channel (21). If the MR damper was in the compression stroke, the fluid flowed in the opposite direction.

In the stretching stroke, when the piston rod was pulled out, part of the recovery chamber (31) of the damper would become empty and the high pressure nitrogen gas in the high pressure nitrogen chamber (13) would push the cylinder piston (15) downward to fill the empty space so that the MR fluid at the lower end of the cylinder piston would enter the compression chamber (28) through the compensation chamber (17) and the lower end annular damping channel (21); in the compression stroke, the MR fluid occupied by the piston rod entered the compensation chamber (17) through the lower end annular damping channel (21) and then pushed the cylinder piston (15) upward to press the nitrogen chamber (13).

In the stretching stroke and compression stroke, when the MR fluid flowed through the upper end annular damping channel (6) and lower end annular damping channel (21), the pressure dropped so that there would be a pressure difference between the recovery chamber and the compression chamber at the upper and lower ends of the piston (30), and it reflected the value of the damping force of the MR damper.

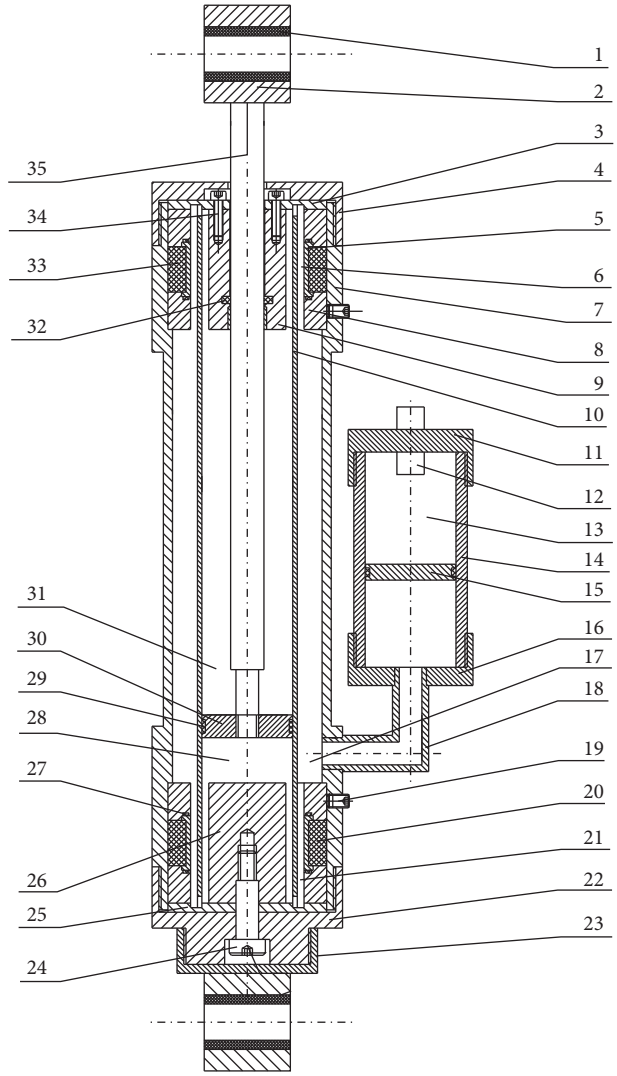

Figure 1: Structural design drawing of an MR damper. 1-ring bushing assembly; 2-upper ring; 3-upper magnetic isolation plate; 4-upper end cover; 5-magnetic isolation ring; 6-upper damping channel; 7-outer cylinder; 8-coil stop; 9-upper stop of piston; 10-inner cylinder; 11-upper end cover of cylinder; 12-charging connector; 13-nitrogen chamber; 14-cylinder block; 15-cylinder piston; 16-lower end cover of cylinder; 17-compensation chamber; 18-conduit; 19-tightening screw; 20-lower coil; 21-lower damping channel; 22-lower end cover; 23-bolt cover; 24-positioning bolt; 25-lower magnetic isolation plate; 26-lower stop of piston; 27-O-type sealing ring; 28-compression chamber; 29-piston seal; 30-piston; 31-recovery chamber; 32-piston rod seal; 33-upper coil; 34-positioning screw; 35-piston rod.

Field coils (33 and 20) were, respectively, arranged on both sides of the upper and lower end annular damping channels (6 and 21), and the magnetic field generated by the coils was perpendicular to the flow direction of MR fluid in the damping channel, which further hindered the flow of MR fluid. As the coil current increased, the magnetic field generated by the coil also gradually increased, causing the viscosity of MR fluid to gradually

increase so that the flow resistance of MR fluid gradually increased, eventually making the damping force of the MR damper gradually increase. Through controlling the intensity of the field coil current, the intensity of damping force of the MR damper can be controlled.

2.2. Characteristics of MR Fluid. MR fluids could be considered as the Newtonian fluid if there was no external magnetic field [36]. Newton fluid characteristics are shown in Figure 2.

The Newton fluid constitutive relationship is shown in the following formula:

$$\tau = \eta\dot{\gamma}, \tag{2}$$

where τ represents the shear stress of MR fluid (Pa), η represents the viscosity (Pa·s), and $\dot{\gamma}$ represents the shear rate (1/s).

In the magnetic field, the MR fluid obtains the shear yield stress and can be considered as the Bingham viscoplastic fluid [37]. The characteristics of the Bingham viscoplastic fluid are shown in Figure 3.

The Bingham viscoplastic model assumed that the MR fluid did not flow before yielding and was approximately considered as a rigid body until the shear stress reached the yield stress of MR fluid, and as the magnetic field intensity increased, the shear yield stress of the MR fluid also gradually increased; after yielding, the MR fluid behaved as the Newton fluid with the shear stress and the shear rate exhibiting a linear relationship. Therefore, under the action of the magnetic field, the MR fluid could be considered to be the Newton fluid with nonzero yield stress, and the constitutive relationship of Bingham viscoplastic fluid is shown in the following formula:

$$\begin{cases} \tau = \tau_B \operatorname{sgn}(\dot{\gamma}) + \eta\dot{\gamma}, & |\tau| \geq \tau_B, \\ \dot{\gamma} = 0, & |\tau| < \tau_B, \end{cases} \tag{3}$$

where τ represents the shear stress of the MR fluid (Pa), τ_B represents the shear yield stress of the MR fluid (Pa), which is controlled by the magnetic field intensity, sgn represents the sign function, η represents the viscosity of the MR fluid (Pa·s), and $\dot{\gamma}$ represents the shear rate of the MR fluid (1/s).

The MR fluid used in this paper was developed by a Chinese company. Its zero-field viscosity was 0.29 Pa·s, and its density was 2.80 g/cm^3. The shear yield stress-magnetic field intensity curve of the MR fluid obtained through experiments is shown in Figure 4. MATLAB fitting toolbox was used to fit the relationship between the shear yield stress curve and the magnetic field intensity. The fitting result is shown in the following formula:

$$\tau_B = -1.567 \times 10^{-11} H^3 + 5.515 \times 10^{-6} H^2 - 0.1206H + 1301, \tag{4}$$

where τ_B represents the shear yield stress of MR fluid (Pa) and H represents the magnetic field intensity (A/m).

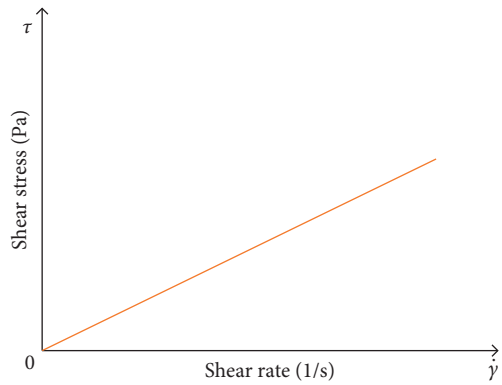

Figure 2: Newton fluid characteristic curve.

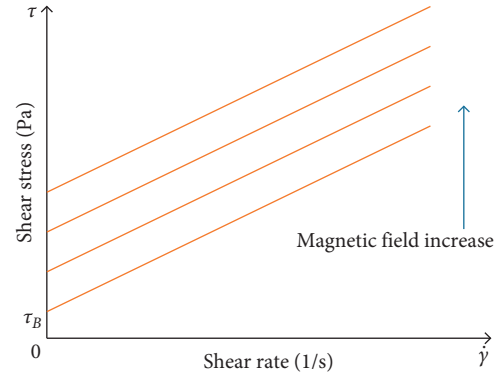

Figure 3: Bingham fluid characteristic curve.

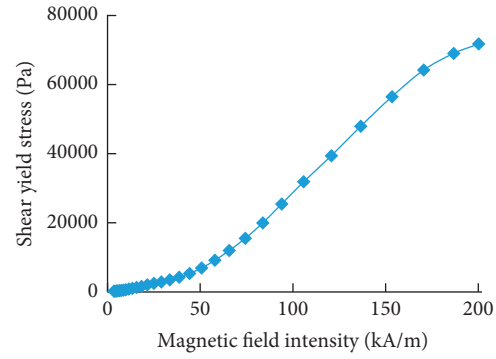

Figure 4: Relationship between shear yield stress of the MR fluid and magnetic field intensity.

3. Establishment of Damper Bond Graph Model

With the development of science and technology, various engineering systems are becoming more and more complex, and they are no longer a single mechanical, electrical, or hydraulic system. There are always engineering systems with multiple energy forms, including electromechanical integration, mechanical fluid integration, or electromechanical fluid integration. It is very difficult to study the dynamic characteristics of such complex system only by using the existing calculation methods involving only one energy field. Therefore, it is necessary to study a unified calculation

method covering multiple energy fields. The bond graph theory method is clear and intuitive in solving the engineering problems existing in machine, electricity, and fluid at the same time.

3.1. Establishment of MR Damper Bond Graph Model

3.1.1. Derivation of the Damping Channel Pressure Drop Formula in Flow Mode. Through comparing the complexity, computational difficulty, and engineering application of the MR fluid constitutive model, the derivation of the damping force of the MR damper based on the Bingham viscoplastic constitutive model is a simple, reliable, and effective MR fluid constitutive model that meets the engineering application precision [38]. The MR damper designed in this paper (as shown in Figure 1) was used under the flow mode. To establish the mathematical model of the damping force of the MR damper, firstly derive the pressure drop of the MR fluid between the two plates in the flow mode based on the Bingham viscoplastic constitutive model. For the convenience of theoretical derivation, the fluid flow in the controllable channel was simplified as the flow between parallel plates, as shown in Figure 5, the fluid in the channel was set to be in the laminar condition, and the side wall effect of the channel was ignored.

τ_B represents the shear yield stress of the MR fluid, which was controlled by the magnetic field intensity(Pa); $\dot{\gamma}$ represents the shear strain rate of the MR fluid (1/s); the x direction represents the flow direction of the MR fluid; u represents the flow velocity of the MR fluid (m/s); y_1 and y_2 represent the dimensions of the plunger shape that the MR fluid presented under the magnetic field (m); h represents the channel gap (m); w represents the channel width (m); L represents the channel length (m); and H represents the magnetic field intensity (kA/m).

After applying a magnetic field perpendicular to the flow direction of the fluid, the MR fluid formed a large number of particle chains with a certain length, diameter, and quantity along the direction of the magnetic field, and as the field intensity increased, the particle chain became longer, its diameter became larger, its number became larger, and the resistance hindering the flow of the MR fluid became larger. Under normal circumstances, the MR fluid between the plates demonstrated a plunger flow pattern and was divided into three regions, one preyield area and two postyield areas near the boundary of the plate. In the preyield area, there was no relative motion between the fluid layers, and the shear stress in this area was zero; in the postyield area, there was relative motion between the fluid layers, and the shear stress between the fluids was related to the intensity of applied field, fluid viscosity, and fluid flow rate.

The N-S equation was used to analyze the force on the fluid. As the channel length was small, the pressure was considered to decrease at a constant velocity in the length direction of the controllable channel, and because of the incompressibility of the fluid, the N-S equation $f_x - (1/\rho)(\partial P/\partial x) + \mu\nabla^2 v_x = (\mathrm{d}v_x/\mathrm{d}t)$ was simplified as

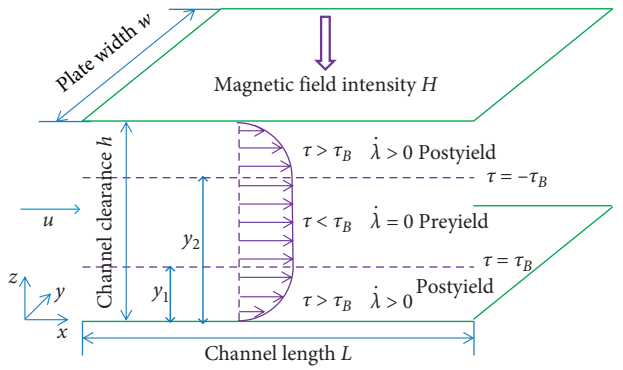

Figure 5: Distribution of velocity of the MR fluid when it flows through a flat plate in the flow mode.

$$\frac{\Delta P_m}{L} = \eta \frac{\mathrm{d}^2 u}{\mathrm{d}y^2}, \tag{5}$$

where ΔP_m represents the pressure drop (Pa) of the controllable channel, L represents the length of the controllable channel (m), η represents the viscosity of the fluid (Pa·s), u represents the velocity in the x direction (m/s), and y represents the coordinate (m) in the direction of the magnetic field.

The shear stress τ of the MR fluid after the magnetic field is added which can be expressed as

$$\tau = \tau_B \mathrm{sgn}\left(\frac{\mathrm{d}u}{\mathrm{d}y}\right) + \eta \frac{\mathrm{d}u}{\mathrm{d}y}, \tag{6}$$

where τ_B represents the shear yield stress (Pa), sgn represents the sign function, $\mathrm{d}u/\mathrm{d}y$ represents the shear strain rate of the MR fluid (1/s), and η represents the viscosity of the MR fluid (Pa·s).

The distribution function of the shear stress obtained is

$$\tau = \begin{cases} \tau_B + \eta \dfrac{\mathrm{d}u_1}{\mathrm{d}y}, & y \in [0, y_1], \\ \tau_B, & y \in [y_1, y_2], \\ -\tau_B + \eta \dfrac{\mathrm{d}u_3}{\mathrm{d}y}, & y \in [y_2, h], \end{cases} \tag{7}$$

where u_1 and u_3, respectively, represent the velocity (m/s) of the MR fluid in the domains $[0, y_1]$, $[y_2, h]$.

Under the action of the magnetic field, the MR fluid is considered to be the Bingham viscoplastic fluid, and the viscosity of the MR fluid is

$$\eta = \frac{\eta_0 + \tau_B}{\mathrm{d}u/\mathrm{d}y}, \tag{8}$$

where η_0 represents the zero-field viscosity of the MR fluid, and the boundary condition is

$$\begin{cases} u_1(0) = u_3(h) = 0; & u_2 = \text{constant}, \\ \dfrac{\mathrm{d}u_1}{\mathrm{d}y}\Big|_{y=y_1} = \dfrac{\mathrm{d}u_3}{\mathrm{d}y}\Big|_{y=y_2} = 0; & \dfrac{\mathrm{d}u_2}{\mathrm{d}y} = 0. \end{cases} \tag{9}$$

Substituting formulae (7) and (8) into formula (5), combined with the boundary condition (9), the functional relationship of the velocity distribution in the controllable channel under the action of the magnetic field can be obtained:

$$u(y) = \begin{cases} -\dfrac{\Delta P_m}{\eta_0 L}\left(\dfrac{1}{2}y^2 - y_1 y\right), & y \in [0, y_1], \\ \dfrac{\Delta P_m}{2\eta_0 L}y_1^2, & y \in [y_1, y_2], \\ -\dfrac{\Delta P_m}{\eta_0 L}\left[\dfrac{1}{2}\left(y^2 - h^2\right) - y_2(y-h)\right], & y \in [y_2, h]. \end{cases} \tag{10}$$

Because of the symmetry of the fluid flow in the channel,

$$y_1 + y_2 = h. \tag{11}$$

Thus, the force balance in the plunger domain is analyzed:

$$\Delta P_m(y_2 - y_1) = 2\tau_B L. \tag{12}$$

Formulae (11) and (12) are combined to obtain *the expressions of* y_1 and y_2:

$$\begin{cases} y_1 = \dfrac{1}{2}h - \dfrac{L\tau_B}{\Delta P_m}, \\ y_2 = \dfrac{1}{2}h + \dfrac{L\tau_B}{\Delta P_m}. \end{cases} \tag{13}$$

Fluid flow Q_m(m^3/s) through the controllable channel is calculated using the following formula:

$$Q_m = \int wu(y)\mathrm{d}y = \sum_{i=1}^{3}\int wu_i(y)\mathrm{d}y. \tag{14}$$

Substitute formulae (10) and (13) into formula (14) to obtain the fluid flow rate of the controllable channel Q_m:

$$Q_m = \frac{\Delta P_m}{12\eta_0 l}wh^3 - \frac{\tau_B}{4\eta_0}wh^2. \tag{15}$$

The pressure drop of the controllable channel ΔP_m is obtained using the following formula:

$$\Delta P_m = \frac{12\eta_0 l}{wh^3}Q_m + \frac{3l}{h}\tau_B. \tag{16}$$

3.1.2. Derivation of Fluid Resistance and Fluid Inductance in Damping Channel. According to the theory of bond graph modeling, analyze the structure of the MR damper designed in this paper in detail and find out 0 node, 1 node, potential source, and flow source. The damping force of the damper was mainly generated by the fluid resistance in the upper- and lower-end damping channels. Therefore, the influence of the fluid resistance and the fluid inductance in the upper- and lower-end damping channels on the damping force of the damper was mainly studied. In addition, the volume compliance of the nitrogen gas in the nitrogen chamber was fully considered. Figure 6 shows the hydraulic model of the MR damper designed in this paper.

According to the knowledge of the bond graph theory, the fluid resistance R_{m1} of the MR fluid in the damping channel at the upper end of the damper can be expressed as

$$R_{m1} = \frac{\Delta P_1}{Q_1}, \tag{17}$$

where ΔP_1 represents the upper-end damping channel pressure drop (Pa) and Q_1 represents the upper-end damping channel flow (m^3/s).

Based on formula (16) for the pressure drop in the damping channel where the MR fluid flows through, combined with the structural size of the MR damper (as shown in Figure 6), the pressure drop ΔP_1 in the upper-end damping channel is

$$\Delta P_1 = \frac{24\eta_0 l}{\pi D h^3}Q_1 + \frac{6l}{h}\tau_B, \tag{18}$$

where η_0 represents the zero-field viscosity (Pa·s) of the MR fluid, the meaning of l, D, and h is as shown in Figure 6, and τ_B represents the shear yield stress (Pa) of the MR fluid.

The flow rate Q_1 flowing through the upper-end damping channel is

$$Q_1 = \left(A_p - A_r\right)v, \tag{19}$$

where A_p represents the piston area (m^2), A_r represents the piston rod area (m^2), and v represents the piston motion velocity (m/s^2).

The fluid resistance R_{m1} in the upper-end damping channel obtained by substituting formulae (18) and (19) into (17) is

$$R_{m1} = \frac{24\eta_0 l}{\pi D h^3} + \frac{6l}{\left(A_p - A_r\right)vh}\cdot\tau_B. \tag{20}$$

Because of different magnetic field intensities on both sides of the inner cylinder of the damper in upper-end damping channel, the shear stress of the fluid is also different. The fluid resistance R_{m1} in the upper-end damping channel obtained by substituting the shear yield stress of the MR fluid on both sides in formula (20) is

$$R_{m1} = \frac{24\eta_0 l}{\pi D h} + \frac{3l}{\left(A_p - A_r\right)vh}\left(\tau_{AB} + \tau_{CD}\right), \tag{21}$$

where τ_{AB} represents the shear yield stress of the AB segment MR fluid (Pa) and τ_{CD} represents the shear yield stress of the CD segment MR fluid (Pa).

According to the relationship between the shear yield stress of the MR fluid and the magnetic field intensity, as shown in Figure 4, its shear yield stress is as follows:

$$\tau_B = -1.567\times10^{-11}H^3 + 5.515\times10^{-6}H^2 - 0.1206H + 1301, \tag{22}$$

where H represents the magnetic field intensity (A/m).

The number of turns of the coils of the damper at the upper- and lower-end damping channel is designed to be 200. According to test data of the magnetic field intensity at the upper and lower damping channels, the magnetic field intensity, H_{AB} and H_{CD}, of the AB segment and CD segment of the damping channel are, respectively,

$$H_{AB} = \frac{NI}{2h + 0.002823}, \tag{23}$$

$$H_{CD} = \frac{NI}{2.012h + 0.005078}, \tag{24}$$

where N represents the number of turns of the coil, I represents the current (A), and h represents the channel clearance (m). Substitute formulae (23) and (24) into (22) to obtain the shear yield stress of the AB segment and CD segment of the damping channel.

The fluid inertia (I_{m1}) of the upper-end damping channel MR fluid is

$$I_{m1} = \rho \frac{L}{A} = \rho \frac{2l}{\pi D h}, \tag{25}$$

where ρ represents the MR fluid density (kg/m^3), L represents the channel length (m), and A represents the channel area (m^2).

Similarly, the fluid resistance R_{m2} of the MR fluid in the damping channel at the lower end of the damper is

$$R_{m2} = \frac{24\eta_0 l}{\pi D h^3} + \frac{3l}{A_p v h}(\tau_{AB} + \tau_{CD}), \tag{26}$$

where the numerical value and meaning of τ_{AB} and τ_{CD} are the same as in formula (7).

The lower-end damping channel fluid inertia I_{m2} is

$$I_{m2} = \rho \frac{L}{A} = \rho \frac{2l}{\pi D h}. \tag{27}$$

The nitrogen chamber volume compliance (C_g) can be expressed as

$$C_g = \frac{V_0}{P_0 n}, \tag{28}$$

where V_0 represents the volume (m^3) of the nitrogen chamber when the piston rod is in the intermediate stroke, P_0 represents the nitrogen pressure (Pa) when the piston rod is at the intermediate stroke, and n represents the heat transfer ratio.

3.1.3. Establishment of MR Damper Bond Graph Model. According to the theoretical modeling method of bond graph, through the structure of the MR damper designed in this paper (as shown in Figure 1), the bond graph model is established as shown in Figure 7. Given an initial velocity $\dot{x}_p$ current source and internal friction F_r potential source of the damper at the damper piston and according to the modeling method of mechanical hydraulic system in bond graph theory, the pressure at the upper and lower ends of the piston was different during the operation of damper; thus, two 0 nodes were established, and it was assumed that the pressure

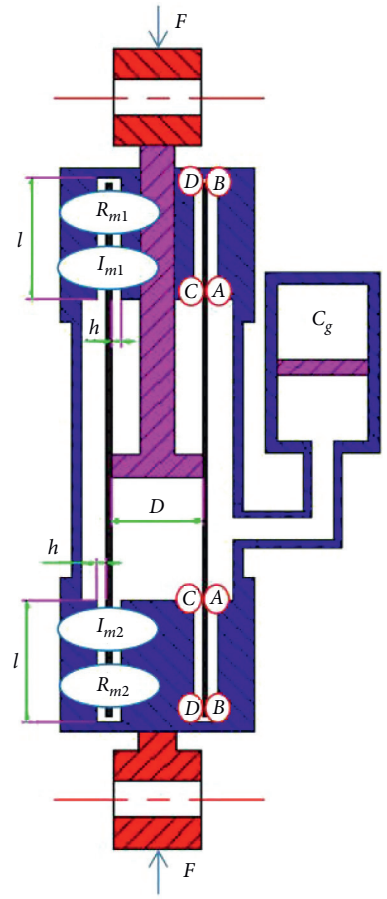

Figure 6: Hydraulic model of the MR damper. D represents the piston diameter (m), l represents the length (m) of one side of the damping channel, h represents the clearance (m) of the damping channel, R_{m1} and R_{m2}, respectively, represent the fluid resistance (N·s/m^5) in the upper and lower damping channels, I_{m1} and I_{m2}, respectively, represent the fluid inductance (N·s^2/m^5) in upper and lower damping channels, C_g represents volume compliance of the nitrogen gas chamber (m^5/N), and F represents damping force of the damper (N).

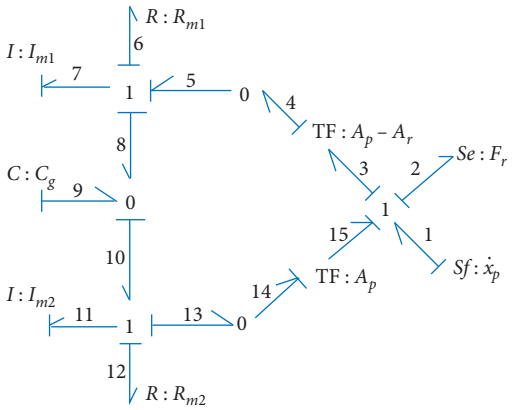

Figure 7: Bond graph model of the MR damper.

at the upper and lower ends of the piston was uniformly distributed; 0 node was established under the nitrogen chamber piston and in the fluid zone between the inner and

outer cylinders, assuming that the pressure distribution was uniform in this zone. The nitrogen chamber volume flexibility was connected to 0 node; in the damping channel at the upper and lower ends, the flow rate of the MR fluid changed significantly, so 1 node was established, and the fluid resistance and fluid sensation of damping channel fluid were, respectively, connected to 1 node; the fluid pressure and force were converted by using a TF converter in the mechanical part and hydraulic part.

Composition rules of inertial element:

$$f_7 = \frac{p_7}{I_7} = \frac{P_{m1}}{I_{m1}}, \tag{29}$$

$$f_{11} = \frac{p_{11}}{I_{11}} = \frac{P_{m2}}{I_{m2}}, \tag{30}$$

where P_{m1} and P_{m2}, respectively, represent the pressure momentum (Pa·s) of the MR fluid for the damping channel at the upper and lower ends.

Composition rules of capacitive element:

$$e_9 = \frac{q_9}{c_9} = \frac{V_g}{C_g}, \tag{31}$$

where V_g represents the nitrogen chamber volume (m^3) and C_g represents the nitrogen chamber volume flexibility (m^5/N).

Composition rules of resistive element:

$$e_6 = R_6 \cdot f_6 = R_{m1} \cdot f_6, \tag{32}$$

$$e_{12} = R_{12} \cdot f_{12} = R_{m2} \cdot f_{12}. \tag{33}$$

Composition rules of 0 node:

$$\begin{cases} e_4 = e_5, \\ f_4 = f_5, \end{cases} \tag{34}$$

$$\begin{cases} e_{14} = e_{13}, \\ f_{14} = f_{13}, \end{cases} \tag{35}$$

$$\begin{cases} e_8 = e_9 = e_{10}, \\ f_{10} = f_8 + f_9. \end{cases} \tag{36}$$

Composition rules of 1 node:

$$\begin{cases} f_1 + f_2 = f_3 + f_{15}, \\ e_1 + e_{15} = e_2 + e_3, \end{cases} \tag{37}$$

$$\begin{cases} f_5 + f_6 = f_7 + f_8, \\ e_5 + e_6 = e_7 + e_8, \end{cases} \tag{38}$$

$$\begin{cases} f_{10} + f_{11} = f_{12} + f_{13}, \\ e_{10} + e_{11} = e_{12} + e_{13}. \end{cases} \tag{39}$$

Composition rules of the converter:

$$\begin{cases} e_3 = \left(A_p - A_r\right) \cdot e_4, \\ f_4 = \left(A_p - A_r\right) \cdot f_3, \end{cases} \tag{40}$$

$$\begin{cases} e_{15} = A_p \cdot e_{14}, \\ f_{14} = A_p \cdot f_{15}. \end{cases} \tag{41}$$

In the aforementioned formula, e and f represent the potential variables and flow variables of the system, respectively. The potential variables and flow variables of the mechanical system are force and velocity, respectively, while the potential variables and flow variables of the hydraulic system are pressure and flow, respectively.

The damping force of the damper is related to the pressure difference between the upper and lower ends of the piston. The damping force F of the damper is obtained by sorting out formula (29)~(41) as

$$F = F_r \cdot \operatorname{sgn}\left(\dot{x}_p\right) - \frac{A_r^2}{C_g} \cdot x_p + \left[R_{m1}\left(A_p - A_r\right) + R_{m2}A_p^2\right] \cdot \dot{x}_p + \left[I_{m1}\left(A_p - A_r\right) + I_{m2}A_p^2\right] \cdot \ddot{x}_p, \tag{42}$$

where F_r represents the internal friction (N) of the MR damper.

Substitute formulas (21), (25), (26), and (27) into (42) to obtain the formula of damping force for the MR damper:

$$F = F_r \cdot \operatorname{sgn}\left(\dot{x}_p\right) - \frac{A_r^2}{C_g} \cdot x_p + \frac{24\eta_0 l}{\pi D h^3}\left[\left(A_p - A_r\right)^2 + A_p^2\right] \cdot \dot{x}_p + \rho\frac{2l}{\pi D h}\left[\left(A_p - A_r\right) + A_p^2\right] \cdot \ddot{x}_p + \left[\frac{3l\left(A_p - A_r\right)}{h} + \frac{3lA_p}{h}\right] \cdot \left(\tau_{AB} + \tau_{CD}\right) \cdot \operatorname{sgn}\left(\dot{x}_p\right). \tag{43}$$

Formula (43)of damping force shows that the damping force of the MR damper was related to factors such as the damper displacement, velocity, acceleration, current, zero-field viscosity of fluid, nitrogen chamber volume flexibility (related to nitrogen pressure), piston diameter, channel clearance, channel length, piston diameter, piston rod diameter, fluid density, and frictional force, wherein the acceleration item represents the inertial force of MR fluid flow.

Different from the parametric model and nonparametric model, the damping force model of the MR damper in this paper was a physical model directly based on the constitutive relation of Bingham viscoplastic MR fluid, the fluid mechanics laws, and bond graph theory.

3.2. Simulation of the Damping Force of MR Damper. The structure parameters of the MR damper in this paper were designed in accordance with the damping force value, the mounting dimensions, and the working stroke required by a military vehicle in China. Among them, piston diameter, piston rod diameter, volume of the nitrogen chamber, nitrogen pressure, length of the damping channel, and turns per coil were determined according to the damping force required by the actual vehicle model, the magnetic field simulation, and the calculation formula of the damping force (43); the length of the cylinder was determined according to the working stroke of the damper of the actual vehicle model; to avoid the MR fluid being blocked in the channel, the size of the channel gap was determined to be 1.5 mm by referring to the domestic and foreign literature. The fluid developed by a Chinese company was selected for the density and zero-field viscosity of the MR fluid, and the internal friction of the damper was determined to be 200 N by referring to the domestic and foreign literature.

3.2.1. Determination of Piston Diameter. The formula for determining the piston diameter of the damper in design is

$$D = \sqrt{\frac{4F_{\max}}{\pi[P]\left(1-\lambda^2\right)}}, \tag{44}$$

where D represents the piston diameter (m), $F_{\max}$ represents the maximum unloading force of the stretching stroke of MR damper(N), and $[P]$ represents the maximum allowable pressure (Pa) in the working cylinder, 3 to 5 MPa is generally set for MR dampers. λ represents the ratio of the diameter of the piston rod to the diameter of the piston cylinder of the MR damper, $\lambda = 0.4$ to 0.5 is set for the double-cylinder damper, and $\lambda = 0.3$ to 0.35 is set for the single-cylinder damper; combined with the actual engineering practice, the maximum allowable pressure in the working cylinder of the MR damper $[P]$ is set to be 5.5 MPa, λ was set to be 0.4, $F_{\max}$ is set to be 6000 N, and the piston diameter calculated using formula (44) is

$$D = \sqrt{\frac{4F_{\max}}{\pi[P]\left(1-\lambda^2\right)}} = \sqrt{\frac{4\times 6000}{\pi\times 5.5\times\left(1-0.4^2\right)}} = 40.67\ \text{mm}. \tag{45}$$

According to the automotive standard QC/T491-1999, the inner diameter of the inner cylinder of the MR damper is selected to be 40 mm and the outer diameter to be 50 mm.

3.2.2. Determination of the Diameter of Piston Rod. The diameter of the piston rod is $d = D\times\lambda = 40.67\times 0.4 = 16.27$ mm. Considering the allowable stress of the piston rod, combined with the actual engineering practice, the diameter of the piston rod in this paper is selected to be 15 mm and the intensity of the piston rod is checked using the following formula:

$$\sigma_{\max} = \frac{F_{\max}}{\pi d^2/4} = \frac{6000}{3.14\times 0.015^2/4} = 33.97\ \text{MPa} < [\sigma] = 170\ \text{MPa}, \tag{46}$$

where $[\sigma]$ represents the allowable stress of the piston rod.

Because of the limited space, the design process of other parameters is no longer detailed. The structural parameters of the MR damper designed in this paper are shown in Table 1.

3.2.3. Simulation Results. Substitute the parameters in Table 1 into the damping force model of the MR damper (formula (43)) to conduct simulation analysis of the damping force of the MR damper. Simulation conditions of the MR damper were determined according to *Automobile Shock Absorber Technique Requirements and Test Methods* of QC/T 491-2018, as shown in Table 2. The motion velocities of the piston were selected as 0.052 m/s, 0.13 m/s, 0.26 m/s, 0.39 m/s, 0.52 m/s, 1.04 m/s, 1.2 m/s, and 1.5 m/s, respectively. In order to study the performance characteristics of the damper at different velocities, the fixed vibration amplitude was selected for the general bench test, and then different excitation frequencies of the bench were determined according to the motion velocity of the damper piston. According to the damper bench test standard of China QC/T 491-2018, the excitation amplitude is selected as 25 mm and sine wave excitation was selected as the bench excitation. The excitation frequencies were 0.33 Hz, 0.83 Hz, 1.66 Hz, 2.48 Hz, 3.33 Hz, 6.62 Hz, 7.64 Hz, and 9.55 Hz, respectively, and the excitation accelerations were 0.11 m/s^2, 0.68 m/s^2, 2.72 m/s^2, 6.06 m/s^2, 10.93 m/s^2, 43.21 m/s^2, 57.55 m/s^2, and 89.92 m/s^2, respectively.

Figure 8 is the force-displacement characteristic of the MR damper at different currents with an excitation amplitude of 25 mm and an excitation frequency of 1.66 Hz and 6.62 Hz. It could be seen that, under the simulation conditions, the larger the current, the larger the area enclosed by force-displacement characteristic, indicating that the MR damper consumed more work.

The damping force at different currents has been simulated at different velocities of the MR damper to obtain its force-velocity characteristic. As shown in Figure 9, it could be seen that, at the same velocity, the damping force of the damper increased with the increase of current. Between 0 and 0.5 A, the damping force increases slowly, and when the current was between 0.5 and 2 A, the amplification of damping force was larger. Meanwhile, since the structural design of the upper and lower ends of damper was the same, the amplitudes of tensile damping force and compression damping force were basically the same.

4. Bench Test Verification

4.1. Test Method. According to *Automobile Shock Absorber Technique Requirements and Test Methods* of QC/T 491-2018, the actuator output waveform was selected as sinusoidal waveform and the vibration amplitude was selected as 25 mm. The force-displacement characteristic and force-velocity characteristic curves of the damper at different velocities were obtained by changing the excitation frequency. The test adopted German SCHENCK hydraulic

bench, and the data acquisition adopted German dSPACE DS1103 card. The detailed steps are as follows:

(1) As shown in Figure 10, the MR damper was mounted on the actuator shaft of a SCHENCK actuator through lifting lugs and clamps, the lower end was mounted on the ground by clamps, and each part was fastened by bolts

(2) The nitrogen cylinder was connected to the damper nitrogen chamber by the pressure gauge, and the pressure of nitrogen chamber was adjusted by the pressure gauge

(3) The positive and negative poles of constant current source were connected to the joints on both ends of the MR damper field coil

(4) As shown in Figure 11, the ports DS1103ADC_1 and DS1103ADC_2 of dSPACE DS1103 card were, respectively, connected with the force and displacement ports of the SCHENCK control cabinet, and the signals of damper displacement and damping force were collected

(5) The actuator was adjusted to the displacement zero point

(6) The amplitude, excitation frequency, and so on of the SCHENCK actuator were set through the control cabinet, and the data with dSPACE were recorded

(7) Steps 5 and 6 were repeated, the field coil current was changed, and the force-displacement characteristic and force-velocity characteristic curves at different currents and excitation frequencies were obtained.

4.2. Test Results. In order to verify the correctness of theoretical simulation results for the damping force of MR damper, the MR damper was verified by bench test, and the test conditions and simulation conditions were consistent, as shown in Table 2.

The force-displacement characteristic and the force-velocity characteristic curves of various working conditions are shown in Figures 12 and 13, respectively. It could be seen that the theoretical value was consistent with the test value in size and trend. Because of the instability of the bench itself, the existence of error in bench sensor test precision, and the errors in the manufacturing and installation process of the MR damper, there was certain fluctuation in the data. During the working process of the MR damper, there was certain frictional force, which could not be accurately measured. The frictional force in the model was an estimated value; thus, there were certain errors in the simulation and test. According to the maximum error statistics of the simulation value and test value under different working conditions, the damping force error was 20 N and the maximum error was 7.2% when the current was 0 A and the piston velocity was 0.052 m/s; as the current increased, the error did not change much. The maximum difference between the simulation value of damping force and the test value was less than 180N, and the total error was below 6.8%.

Table 1: Structural parameters of the MR damper.

Parameter	Numeric value
Coil turns, N	200
Channel clearance, h (m)	0.0015
Single-side damping channel length, l (m)	0.03
Piston diameter, D (m)	0.04
Diameter of the piston rod, d (m)	0.015
Density of the MR fluid, ρ (kg/m^3)	2800
Zero-field viscosity of the MR fluid, η_0 (Pa·s)	0.29
Nitrogen pressure, P_0 (MPa)	0.6
Frictional force, F_r (N)	200
Nitrogen chamber volume flexibility, C_g (m^3/Pa)	$6.28E-11$

Table 2: Simulation conditions.

Parameters	Numeric value
Input current (A)	0, 0.25, 0.5, 0.75, 1, 1.25, 1.5, 1.75, 2
Excitation frequency (Hz)	0.33, 0.83, 1.66, 2.48, 3.33, 6.62, 7.64, 9.55
Excitation amplitude (m)	0.025
Velocity (m/s)	0.052, 0.13, 0.26, 0.39, 0.52, 1.04, 1.2, 1.5
Acceleration (m/s^2)	0.11, 0.68, 2.72, 6.06, 10.93, 43.21, 57.55, 89.92

5. Influence of MR Fluid Inertial Force on Damping Force of MR Damper

Lee and Choi [35] established a physical model of MR damper containing the piston, motion displacement, velocity, and shear stress of the MR fluid while neglecting the inertial force of the MR fluid.

The MR damper model studied in this paper concluded not only the piston motion displacement, velocity, and shear stress of the MR fluid but also the acceleration term, which represents the inertial force of MR fluid flow.

The relationship between the acceleration term and the piston motion acceleration in the MR damper model is shown in Figure 14. When the excitation frequency was 3.33 Hz, the piston motion acceleration was 10.93 m/s^2 and the damping force of the acceleration term reached 25.4 N. When the excitation frequency was 9.55 Hz, the acceleration of the piston motion was 89.92 m/s^2 and the damping force of the acceleration term reached 209.5 N.

In order to study the influence of the inertial force of the MR fluid on the damping force, this paper analyzed the influence of the inertial force of the MR fluid on the damping force under different working conditions. The comparison of characteristic curves of the MR damper with or without acceleration term in the damping force model of the MR damper at different excitation frequencies and currents was simulated, respectively. The characteristic curves included force-acceleration characteristic curve, force-displacement characteristic curve, and force-velocity characteristic curve. The results of simulation comparison are shown in Figures 15–17.

It could be seen from Figures 15–17 that when the excitation frequency was below 3.33 Hz, the force had less influence on the force-acceleration characteristic, the force-displacement characteristic, and the force-velocity

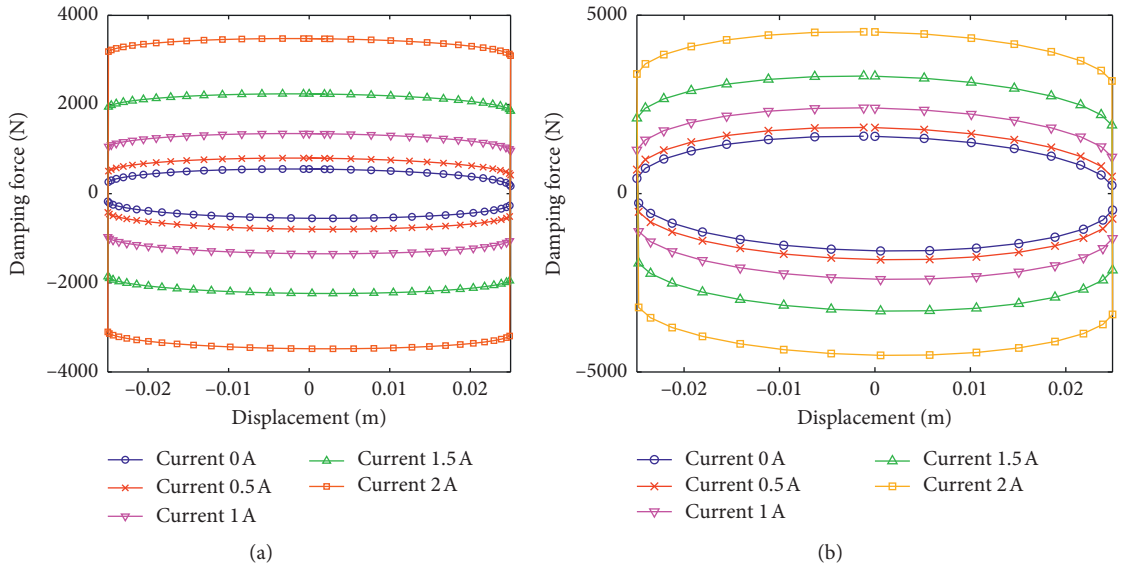

Figure 8: Simulation force-displacement characteristic of the MR damper. (a) 1.66 Hz and (b) 6.62 Hz.

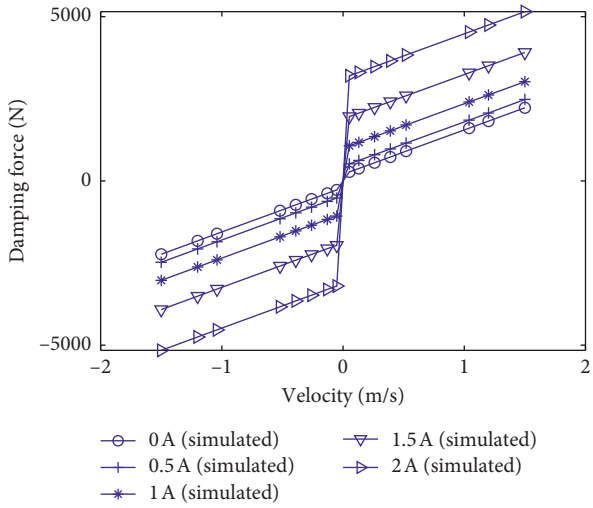

Figure 9: Simulation results of the force-velocity characteristic of the MR damper.

Figure 10: Test bench of MR fluid damper performance.

Figure 11: dSPACE signal collection system.

characteristic of the MR fluid damper and had a great influence on the force-acceleration characteristic, the force-displacement characteristic, and the force-velocity characteristic of the MR fluid when the excitation frequency was beyond 6.62 Hz. In addition, the acceleration term was only related to the acceleration of the piston motion, but not to the current; therefore, at each excitation frequency, the inertial force of the MR fluid had a great influence on the characteristic curve of the MR damper when there was no current, and as the current applied increased, the influence on the force-acceleration characteristic, the force-displacement characteristic, and the force-velocity characteristic of the MR damper decreased gradually.

In order to evaluate the degree of influence of the inertial force of MR fluid on the damping force model, we have carried out the following calculations. The ratio of the maximum difference value ΔF and the damping force value with the acceleration term at maximum difference point $F_{\max}$

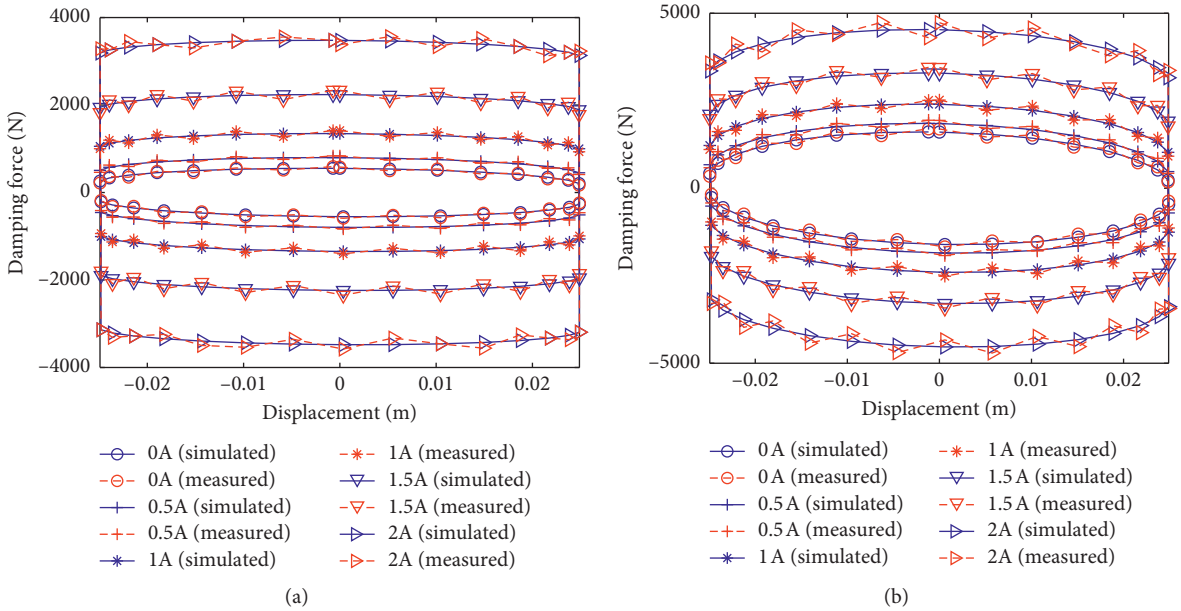

Figure 12: Test results of the force-displacement characteristic of the MR damper. (a) 1.66 Hz and (b) 6.62 Hz.

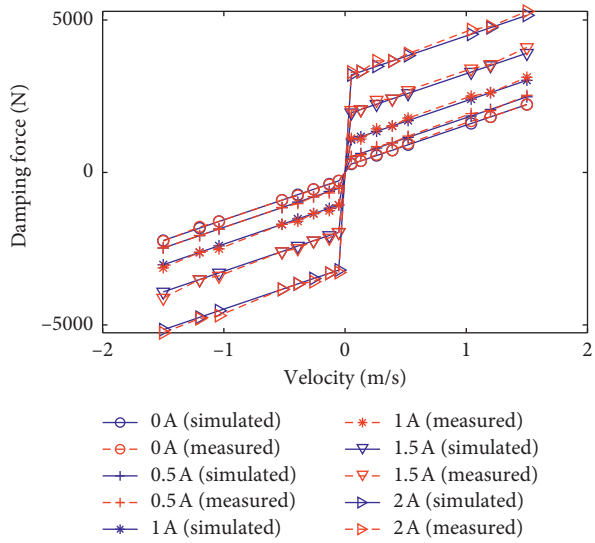

Figure 13: Test results of the force-velocity characteristic of the MR damper.

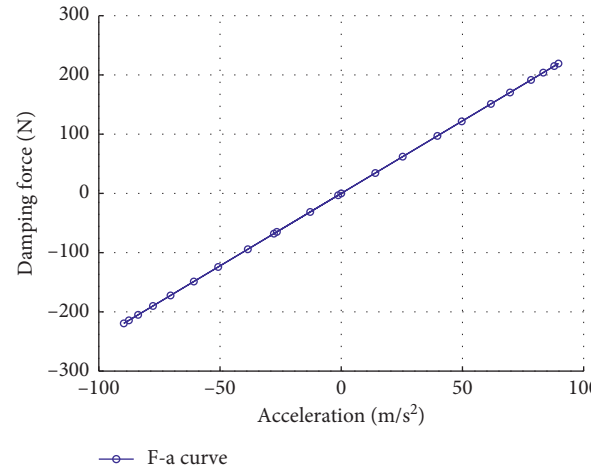

Figure 14: Relationship between MR fluid inertia force and acceleration.

in the force-acceleration characteristic curve r was calculated, and the calculation method is shown in formula (47). Figure 18 shows the values of ΔF and Fmax. The larger the ratio, the greater the degree of influence of the inertia force of the MR fluid on the damping force and vice versa.

The calculation formula is as follows:

$$r = \frac{\Delta F}{F_{\max}} \times 100\%. \quad (47)$$

As can be seen in Table 3, when the excitation frequency was less than or equal to 2.48 Hz, the ratio r was less than 1.29%, which can be ignored; when the excitation frequency was 3.33 Hz, the maximum ratio was 6.87%, the inertial force of the MR fluid had relatively less influence on the damping force of the damper, while when the excitation frequency was 6.62 Hz, the maximum ratio r reached 19.2%. As the excitation frequency increased, the ratio gradually increased. When the excitation frequency was 9.55 Hz, the maximum ratio r reached 35.8%. This shows that when the frequency of the damper is large, the inertial force of the MR fluid has an important influence on the damping force; therefore, considering the inertial force of the MR fluid in the model can greatly improve the accuracy of the model.

6. Study on Sensitivity of Damping Force Parameters

According to the research results of Section 4.2, it could be seen that the single-rod double-cylinder and double-coil MR damper model studied in this paper was correct. Therefore,

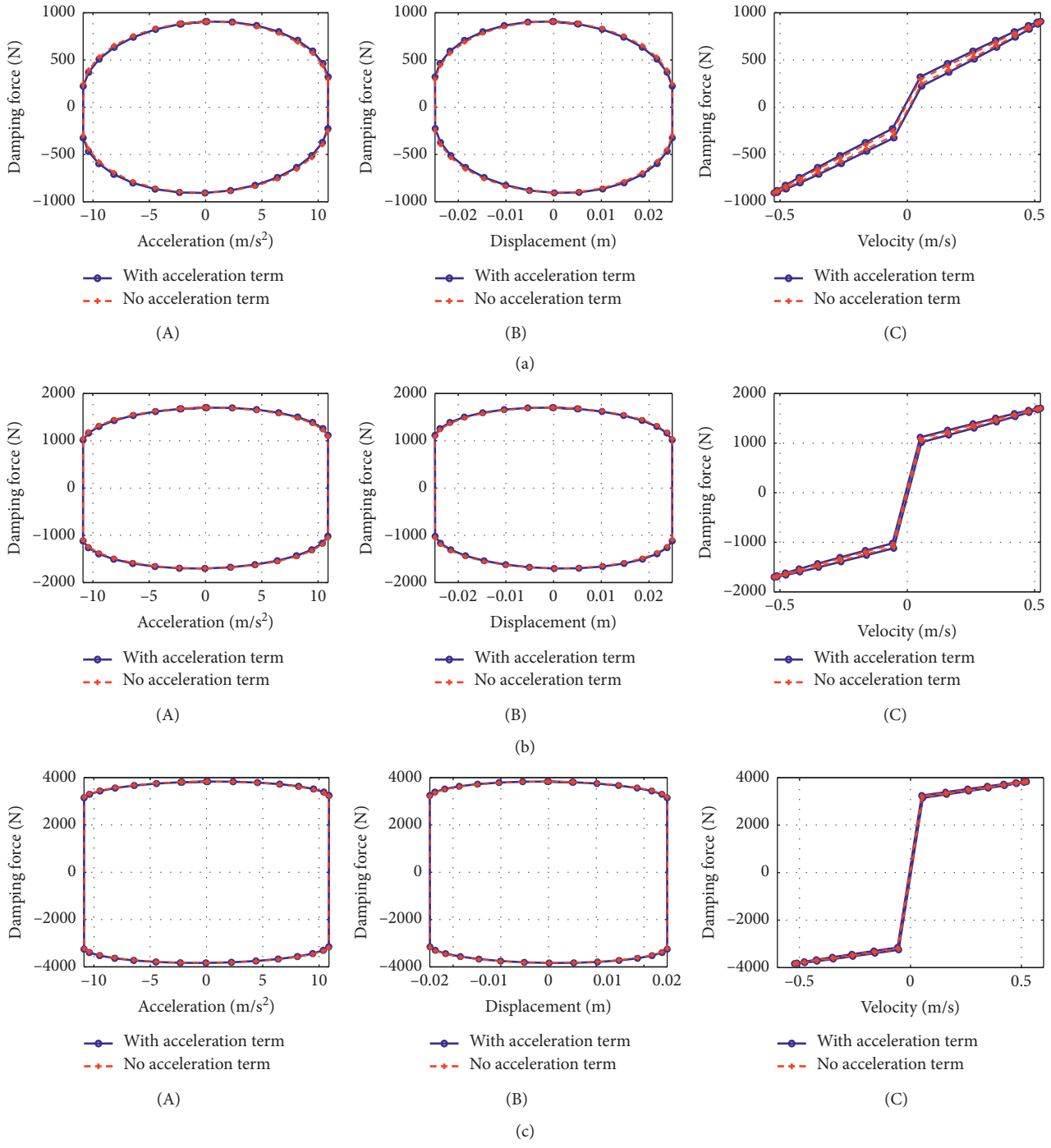

Figure 15: Comparison of characteristic curves with or without acceleration term under 3.33 Hz. (A) Force-acceleration characteristic; (B) force-displacement characteristic; (C) force-velocity characteristic. (a) 0A; (b) 1A; (c) 2A.

the influence rule and sensitivity of key parameters such as energizing current, motion velocity, damping channel clearance, damping channel length, piston diameter, zero-field viscosity of the MR fluid, and nitrogen pressure in the model on the damping force of the damper could be studied based on the theoretical model.

6.1. Influence Rule of Key Parameters on Damping Force

6.1.1. Constraint Conditions. In order to quantitatively study the influence rule of key parameters on damping force in the damping force model of the MR damper, the variation range of key parameters should be firstly determined according to

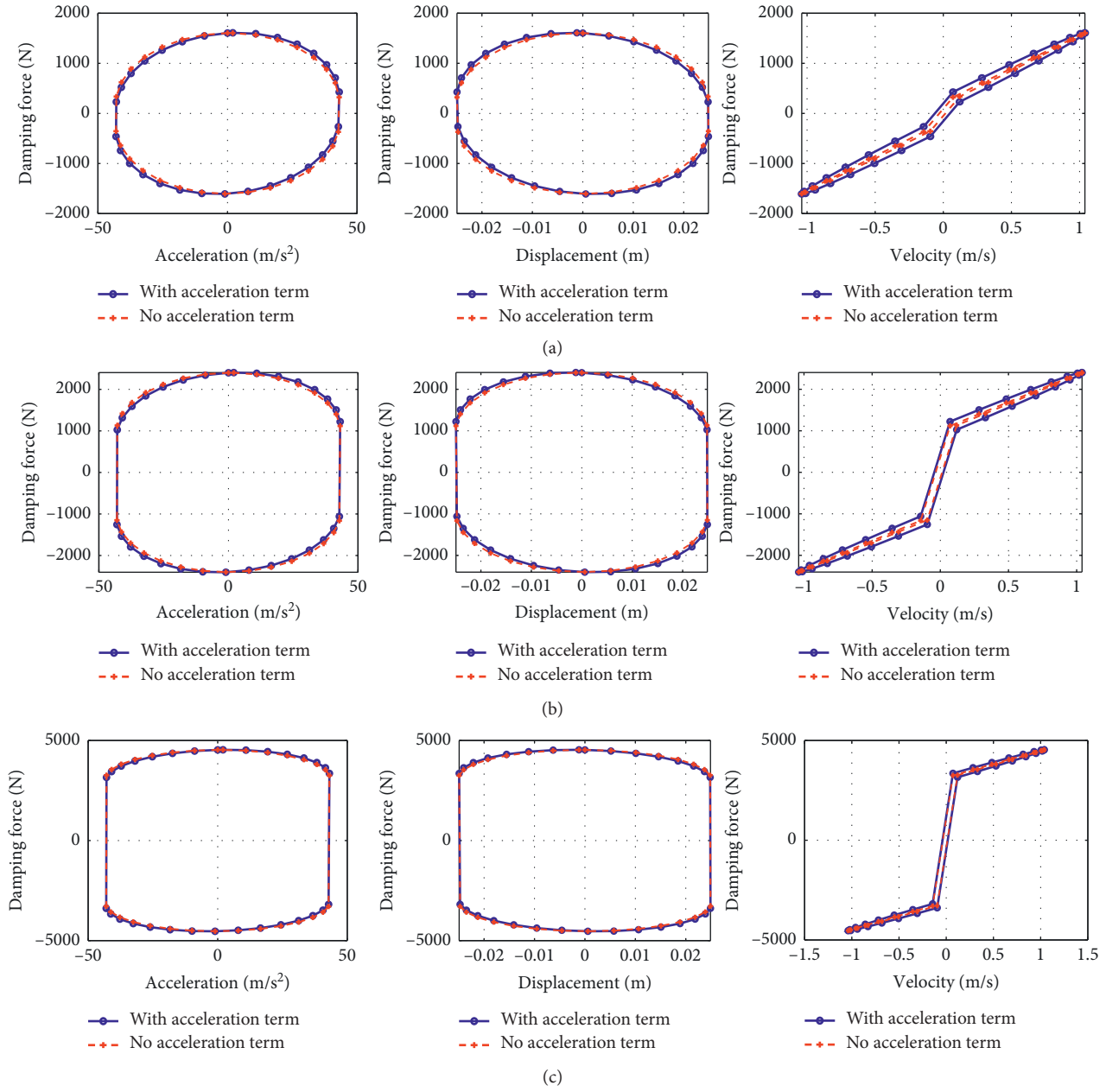

Figure 16: Comparison of characteristic curves with or without acceleration term under 6.62 Hz. (A) Force-acceleration characteristic; (B) force-displacement characteristic; (C) force-velocity characteristic. (a) 0A; (b) 1A; (c) 2A.

the actual structure and working conditions of the MR damper, as shown in Table 4.

6.1.2. Influence of Current and Velocity Variations on Damping Force of Damper. For the influence of current and velocity variations on damping force of the MR damper, the results are shown in Figure 19. It could be seen that the damping force of the damper increased with the increase of current at the same velocity and the amplification was larger. Under the same current, the damping force of the damper increased with the increase of velocity and the amplification was slower.

6.1.3. Influence of Channel Clearance and Current Variation on Damping Force. For the influence of channel clearance and current variation on the damping force of the MR damper, the results are shown in Figure 20. It could be seen that the damping force of the damper decreased with the increase of channel clearance at the same current and the reduction amplitude was larger. Under the same channel clearance, the damping force of the MR fluid damper increased with the increase of current and the amplification was larger.

6.1.4. Influence of Channel Length and Current Variation on Damping Force. For the influence of channel length and

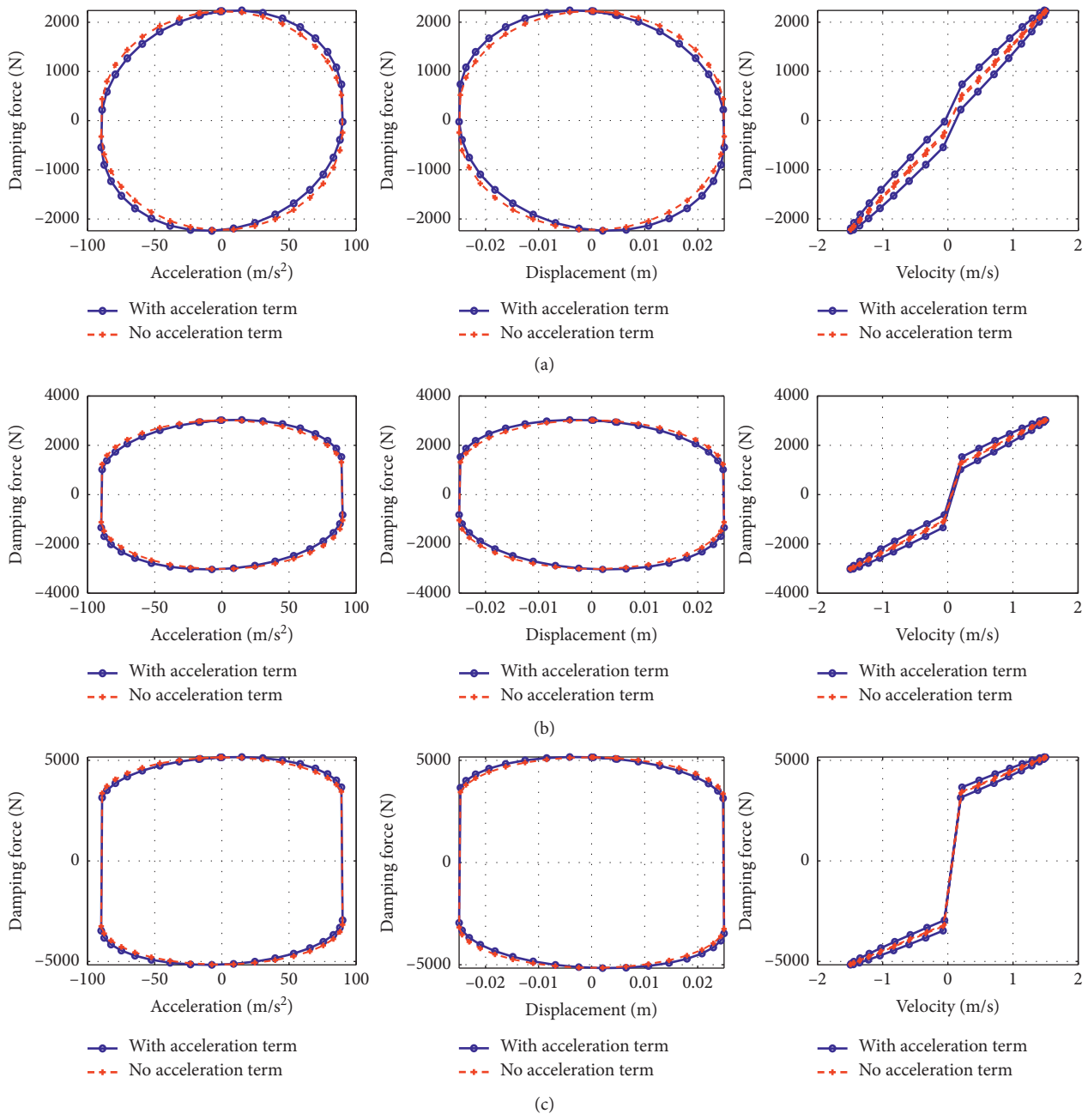

FIGURE 17: Comparison of characteristic curves with or without acceleration term under 9.55 Hz. (A) Force-acceleration characteristic; (B) force-displacement characteristic; (C) force-velocity characteristic. (a) 0A; (b) 1A; (c) 2A.

current variation on the damping force of the MR damper, the results are shown in Figure 21. It could be seen that the damping force of the damper increased with the increase of channel length at the same current. Under the same channel length, the damping force of the MR fluid damper increased with the increase of current and the amplification was larger.

6.1.5. Influence of Piston Diameter and Current Variation on Damping Force. For the influence of piston diameter and current variation on damping force of the MR damper, the results are shown in Figure 22. It could be seen that the damping force of the damper increased with the increase of the piston diameter at the same current and the amplification was larger. Under the same piston diameter, the damping force of the MR fluid damper increased with the increase of current and the amplification was larger.

6.1.6. Influence of Zero-Field Viscosity and Current Variation on Damping Force. For the influence of the zero-field viscosity of the MR fluid and current variation on damping force of the MR damper, the results are shown in Figure 23. It could be seen that the damping force of the damper

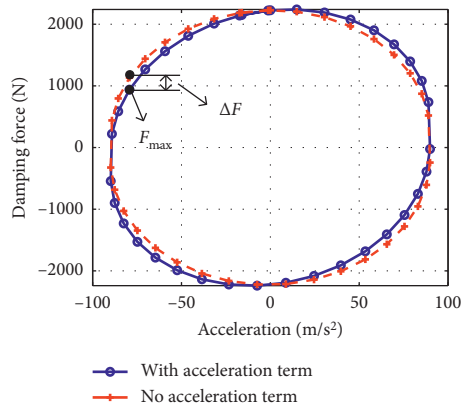

Figure 18: Calculation diagram of the influence degree of MR fluid inertia force.

Table 3: Calculation results of the force-acceleration curves difference percentage.

Frequency (Hz)	Velocity (m/s)	Acceleration (m/s^2)	Input current (A)	Maximum difference value ΔF_{max} (N)	Damping force with acceleration term at maximum difference point F_{max} (N)	Difference ratio r (%)
0.33	0.052	0.11	0	0.1	253.5	0.04
			1	0.1	1048	0.01
			2	0.1	3180	0.003
0.83	0.13	0.68	0	0.8	339	0.24
			1	0.8	1134	0.07
			2	0.8	3265	0.02
1.66	0.26	2.72	0	3.9	466.4	0.83
			1	3.9	1261	0.31
			2	3.9	3393	0.11
2.48	0.39	6.06	0	8	621.2	1.29
			1	8	1424	0.56
			2	8	3555	0.23
3.33	0.52	10.93	0	25.4	369.5	**6.87**
			1	25.4	1164	2.18
			2	25.4	3296	0.77
6.62	1.04	43.21	0	100.2	521.8	**19.2**
			1	100.2	1317	**7.6**
			2	100.2	3448	2.9
7.64	1.2	57.55	0	131.2	632.8	**20.7**
			1	131.2	1428	**9.2**
			2	131.2	3559	3.7
9.55	1.5	89.92	0	209.5	586.6	**35.8**
			1	209.5	1382	**15.2**
			2	209.5	3513	**5.96**

Table 4: Constraint conditions of key parameters.

Independent variable	Constraint conditions						
	Current (A)	Velocity (m/s)	Channel clearance (m)	Channel length (m)	Piston diameter (m)	Zero-field viscosity (Pa·s)	Nitrogen pressure (MPa)
Current	[0, 2 A]	[0.052, 1.5]	0.0015	0.03	0.04	0.29	0.6
Velocity	[0, 2 A]	[0.052, 1.5]	0.0015	0.03	0.04	0.29	0.6
Channel clearance	[0, 2 A]	0.52	[0.001, 0.002]	0.03	0.04	0.29	0.6
Channel length	[0, 2 A]	0.52	0.0015	[0.02, 0.04]	0.04	0.29	0.6
Piston diameter	[0, 2 A]	0.52	0.0015	0.03	[0.03, 0.05]	0.29	0.6
Zero-field viscosity	[0, 2 A]	0.52	0.0015	0.03	0.04	[0.24, 0.34]	0.6
Nitrogen pressure	[0, 2 A]	0.52	0.0015	0.03	0.04	0.29	[0.5, 1]

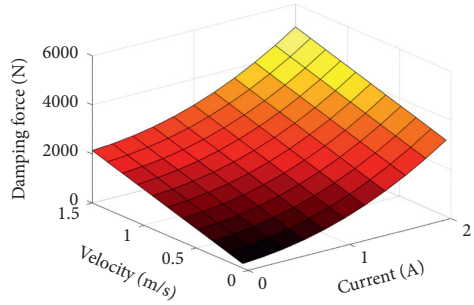

Figure 19: Influence of current variation on damping force.

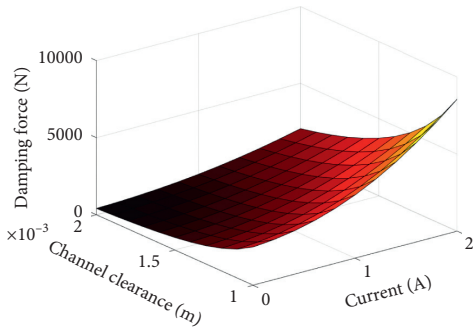

Figure 20: Influence of channel clearance and current variation on damping force.

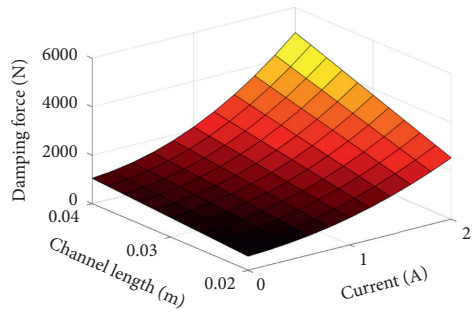

Figure 21: Influence of channel length and current variation on damping force.

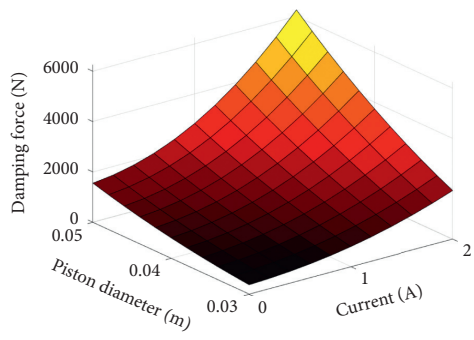

Figure 22: Influence of piston diameter and current variation on damping force.

increased with the increase of zero-field viscosity of the MR fluid at the same current, but the amplification was slow which almost has no influence. Under the same zero-field viscosity of the MR fluid, the damping force of the MR fluid damper increased with the increase of current and the amplification was larger.

6.1.7. Influence of Nitrogen Pressure and Current Variation on Damping Force. For the influence of nitrogen pressure and current variation on damping force of the MR damper, the results are shown in Figure 24. It could be seen that the damping force of the damper increased with the decrease of nitrogen pressure at the same current, but the amplification was slow, which almost had no influence. Under the same nitrogen pressure, the damping force of the MR fluid damper increased with the increase of current and the amplification was larger.

6.2. Sensitivity of the Influence on Damping Force by Various Parameters. Sensitivity of the influence on damping force by various parameters has been defined as the percentage of the variation for damping force of the MR damper in parameter variation ΔF_i to the damping force F_{io} under the median of parameter variation for the MR damper. It was used to measure the influence of this parameter on the damping force of the MR damper, expressed as s, and the expression is as follows:

$$s = \frac{\Delta F_i}{F_{io}} \times 100\%. \tag{48}$$

Substitute the simulation value of Figures 19–24 into formula (48). When studying the sensitivity of the influence on damping force by current variation, select the median of velocity 0.75 m/s, and when studying the sensitivity of the influence on damping force by other parameters, select the median of current 1 A so that the influence degree of each parameter on the damping force of the MR damper could be obtained. As shown in Figure 25, the positive value of sensitivity indicated that the damping force of the MR damper increased as the parameter increased, i.e., positive correlation, and negative value indicated that the damping force of the MR damper decreased as the parameter increased, i.e., negative correlation.

As can be seen from Figure 25,

(1) The influence degree on the damping force of the MR damper successively ranging from the maximum to the minimum was the channel clearance, energizing current, piston diameter, motion velocity, channel length, zero-field viscosity of MR fluid, and nitrogen pressure. In the design of the damping force of the MR damper, the above parameters could be adjusted to quickly achieve the required damping force.

(2) Among them, the sensitivity of the influence on damping force of the MR damper by energizing current and damping channel clearance was the maximum, reaching more than 155%. Increasing current and reducing damping channel clearance were beneficial to the great improvement of the damping force of the damper. However, the channel clearance should not be too small; otherwise, it can

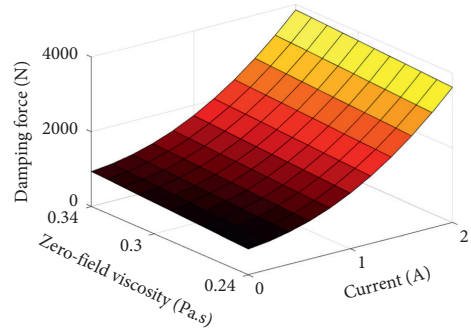

Figure 23: Influence of zero-field viscosity and current variation on damping force.

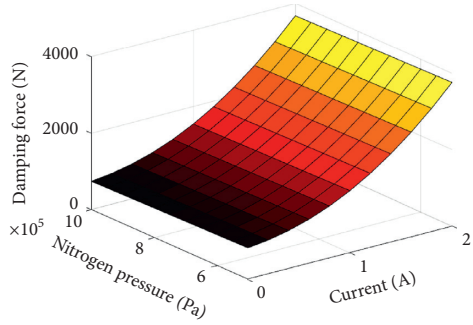

Figure 24: Influence of nitrogen pressure and current variation on damping force.

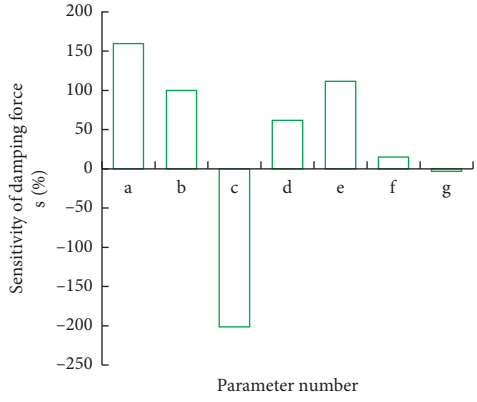

Figure 25: Sensitivity of various parameters to damping force. a, current; b, velocity; c, channel clearance; d, channel length; e, piston diameter; f, zero-field viscosity of MR fluid; g, nitrogen pressure.

easily cause the MR fluid to block in the damping channel.

(3) The zero-field viscosity of the MR fluid and nitrogen pressure almost had no influence on the damping force of the MR damper, but the viscosity should not be too high when selecting the zero-field viscosity of the MR fluid; otherwise, it will also easily cause damping channel blocking of the damper. The nitrogen pressure should not be too small; otherwise, it will easily cause concave force-displacement characteristic curve.

7. Conclusions

(1) The single-rod double-cylinder and double-coil MR damper model established based on the multifield modeling method bond graph theory and adopted in this paper can not only consider the parameters such as damper displacement and velocity but also consider the influence of inertial force of MR fluid, i.e., the acceleration item in the model on damping force, which improved the model precision. Experimental verification showed that the modeling method was correct.

(2) The damping force model of the MR damper studied in this paper was compared with that of the damper without considering the inertia force of the MR fluid and the influence of the inertia force of the MR fluid on the damping force of the MR damper was analyzed. When the excitation frequency was less than or equal to 2.48 Hz, the ratio r was less than 1.29%, which can be ignored; when the excitation frequency was 3.33 Hz, the maximum ratio r was 6.87%, the inertial force of MR fluid has relatively less influence on the damping force of the damper. When the excitation frequency was 6.62 Hz, the maximum ratio r reached 19.2%. As the excitation frequency increased, the ratio gradually increased. When the excitation frequency was 9.55 Hz, the maximum ratio r reached 35.8%. This shows that when the frequency of the damper is large, the inertial force of the MR fluid has an important influence on the damping force; therefore, considering the inertial force of the MR fluid in the model can greatly improve the accuracy of the model.

(3) Through the theoretical model, the influence degree of key parameters on the damping force of the damper was studied, ranging from the maximum to the minimum; it has been the channel clearance, energizing current, piston diameter, motion velocity, channel length, zero-field viscosity of the MR fluid, and nitrogen pressure, providing a basis for the adjustment of damping force of the damper.

Data Availability

The data used to support the findings of this study are available from the corresponding author upon request.

Conflicts of Interest

The authors declare that there are no conflicts of interest regarding the publication of this paper.

Acknowledgments

This work was supported by the Henan Science and Technology Project (182102210034) and (192102210063) and National Natural Science Foundation of China (51705468).

References

[1] J. Chen, *Automobile Structure*, China Machine Press, Beijing, China, 2010.

[2] N. M. Wereley, J. U. Cho, Y. T. Choi, and S. B. Choi, "Magnetorheological dampers in shear mode," *Smart Materials and Structures*, vol. 17, no. 1, pp. 1–11, 2008.

[3] C. Wang, S. H. I. Wenku, Y. Zhang et al., "Virtual matching optimization of variable stiffness suspension," *Journal of Hunan University (Natural Sciences)*, vol. 42, no. 4, pp. 19–26, 2015.

[4] Y. Li, D. Song, J. Li et al., "Shock absorber controller of damping-adjustable semi-active suspension for CA6440 light-duty bus," *Journal of Jilin University (Engineering and Technology Edition)*, vol. 34, no. 1, pp. 71–74, 2004.

[5] L. Jiang, *Research on Matching Design and Control of Vehicle Electronic Control Air suspension*, Jinlin University, Changchun, China, 2007.

[6] W. Chen, Z. Wang, and D. Fan, "Adaptive control of semi-active automotive suspension using neural network," *Automotive Engineering*, vol. 20, no. 1, pp. 31–36, 1998.

[7] C. Liao, *Study on Magnetorheological Fluid Damper for Automobile Suspension System*, Chongqing University, Chongqing, China, 2001.

[8] S. Liu, *Studies on the Characteristics of Magnetorheological Adjustable Damper*, Jiangsu University, Zhenjiang, China, 2007.

[9] J. Chen, *Research on Design and Control of Automotive Semi-active Suspension Based on Magneto-Rheological damper*, Hefei University of Technology, Hefei, China, 2010.

[10] F. Liu, Y. Li, and L. Zheng, "Variable universe fuzzy control for the magneto-rheological semi-active suspension in armored vehicles," *Automotive Engineering*, vol. 35, no. 8, pp. 735–739, 2013.

[11] J. Weng, H. Hu, and M. K. Zhang, "Fuzzy semi-active control of vehicle suspension system based on magneto-rheological damper," *Journal of Nanjing University of Technology*, vol. 24, no. 1, pp. 57–61, 2002.

[12] R. Stanway, J. L. Sproston, and N. G. Stevens, "Non-linear modelling of an electro-rheological vibration damper," *Journal of Electrostatics*, vol. 20, no. 2, pp. 167–184, 1987.

[13] S. R. Hong, S. B. Choi, Y. T. Choi, and N. M. Wereley, "Non-dimensional analysis and design of a magneto-rheologicaldamper," *Journal of Sound and Vibration*, vol. 288, no. 4-5, pp. 847–863, 2005.

[14] S. R. Hong, N. M. Wereley, Y. T. Choi, and S. B. Choi, "Analytical and experimental validation of a nondimensional Bingham model for mixed-mode magnetorheological dampers," *Journal of Sound and Vibration*, vol. 312, no. 3, pp. 399–417, 2008.

[15] N. M. Wereley, L. Pang, and G. M. Kamath, "Idealized hysteresis modeling of electrorheological and magneto-rheological dampers," *Journal of Intelligent Material Systems and Structures*, vol. 9, no. 8, pp. 642–649, 1998.

[16] X. Wang and F. Gordaninejad, "Flow analysis of field-controllable, electro- and magneto-rheological fluids using Herschel-Bulkley model," *Journal of Intelligent Material Systems and Structures*, vol. 10, no. 8, pp. 601–608, 1999.

[17] D. Y. Lee, Y. T. Choi, and N. M. Wereley, "Performance analysis of ER/MR impact damper systems using Herschel-Bulkley model," *Journal of Intelligent Material Systems and Structures*, vol. 13, no. 7-8, pp. 525–531, 2002.

[18] B. F. Spencer, S. J. Dyke, M. K. Sain, and J. D. Carlson, "Phenomenological model for magnetorheological dampers," *Journal of Engineering Mechanics*, vol. 123, no. 3, pp. 230–238, 1997.

[19] S.-B. Choi, S.-K. Lee, and Y.-P. Park, "A hysteresis model for the field-dependent damping force of a magnetorheological damper," *Journal of Sound and Vibration*, vol. 245, no. 2, pp. 375–383, 2001.

[20] G. Z. Yao, F. F. Yap, G. Chen, W. H. Li, and S. H. Yeo, "MR damper and its application for semi-active control of vehicle suspension system," *Mechatronics*, vol. 12, no. 7, pp. 963–973, 2002.

[21] H. Komatsu, H. Enomoto, T. Komatsuzaki, and K. Izumi, "Effect of electrically controlled MR-damper on the cornering of small racing car," SAE Technical Papers, 2011.

[22] H. Du, K. Y. Sze, and J. Lam, "Semi-active H_∞ control of vehicle suspension with magneto-rheological dampers," *Journal of Sound and Vibration*, vol. 283, no. 3–5, pp. 981–996, 2005.

[23] A. Dominguez, R. Sedaghati, and I. Stiharu, "Modeling and application of MR dampers in semi-adaptive structures," *Computers and Structures*, vol. 86, no. 3-5, pp. 407–415, 2008.

[24] J. Bajkowski, J. Nachman, M. Shillor, and M. Sofonea, "A model for a magnetorheological damper," *Mathematical and Computer Modelling*, vol. 48, no. 1-2, pp. 56–68, 2008.

[25] M. J. L. Boada, J. A. Calvo, B. L. Boada, and V. Díaz, "Modeling of a magnetorheological damper by recursive lazy learning," *International Journal of Non-linear Mechanics*, vol. 46, no. 3, pp. 479–485, 2011.

[26] J. L. Yao, *Theoretical and Experimental Research on Vehicle Magnetorheological Semi-active Suspension System*, Nanjing Forestry University, Nanjing, China, 2009.

[27] X. C. Guan, P. F. Guo, and J. P. Ou, "Modeling and analyzing of hysteresis Behavior of magneto rheological dampers," *Procedia Engineering*, vol. 14, pp. 2756–2764, 2011.

[28] P. F. Guo, *Research on Mechanical Characteristics and Design Methods of Magnetorheological Fluid Dampers*, Harbin Institute of Technology, Harbin, China, 2011.

[29] L. Zhou, "Neural network emulation of inverse dynamics for a magnetorheological damper," *Journal of Structural Engineering*, vol. 128, pp. 231–239, 2002.

[30] H. Du, J. Lam, and N. Zhang, "Modelling of a magneto-rheological damper by evolving radial basis function networks," *Engineering Applications of Artificial Intelligence*, vol. 19, no. 8, pp. 869–881, 2006.

[31] D. H. Wang and W. H. Liao, "Modeling and control of magnetorheological fluid dampers using neural networks," *Smart Materials and Structures*, vol. 14, no. 1, pp. 111–126, 2005.

[32] K. C. Schurter and P. N. Roschke, "Fuzzy modeling of a magnetorheological damper using ANFIS," in *Proceedings of the Ninth IEEE International Conference on Fuzzy Systems (FUZZ- IEEE 2000 (Cat. No.00CH37063))*, pp. 122–127, San Antonio, TX, USA, May 2000.

[33] H. Wang, "Modeling of magnetorheological damper using neuro-fuzzy system," *Advances in Soft Computing*, vol. 2, pp. 1157–1164, 2009.

[34] H. Wang and H. Hu, "The neuro-fuzzy identification of MR damper," in *Proceedings of the 2009 Sixth International Conference on Fuzzy Systems and Knowledge Discovery*, pp. 464–468, IEEE, Tianjin, China, August 2009.

[35] H.-S. Lee and S.-B. Choi, "Control and response characteristics of a magneto-rheological fluid damper for passenger vehicles," *Journal of Intelligent Materials Systems and Structures*, vol. 11, no. 1, pp. 80–87, 2000.

[36] J. D. Carlson and M. R. Jolly, "MR fluid, foam and elastomer devices," *Mechatronics*, vol. 10, no. 4-5, pp. 555–569, 2000.

[37] F. Omidbeygi and S. H. Hashemabadi, "Experimental study and CFD simulation of rotational eccentric cylinder in a magnetorheological fluid," *Journal of Magnetism and Magnetic Materials*, vol. 324, no. 13, pp. 2062–2069, 2012.

[38] G. A. Dimock, J.-H. Yoo, and N. M. Wereley, "Quasi-steady Bingham biplastic analysis of electrorheological and magnetorheological dampers," *Journal of Intelligent Material Systems and Structures*, vol. 13, no. 9, pp. 549–559, 2002.